J Fluoresc (2015) 25:379–385
DOI 10.1007/s10895-015-1523-3

ORIGINAL PAPER

Fluorescence Quenching N,N-Bis(2,6-Dimethylphenyl) -3,4:9,10-Perylenetetracarboxylic Diimide (BDPD) Laser Dye by Colloidal Silver Nanoparticles

Samy A. El-Daly · Ibrahim A. Salem · Mahmoud A. Hussein · Abdullah M. Asiri

Received: 13 October 2014 / Accepted: 20 January 2015 / Published online: 6 February 2015

Abstract The fluorescence quenching N,N-bis(2,6-dimethylphenyl)-3,4:9,10-perylenetetra-carboxylic diimide (BDPD) by colloidal silver nanoparticles (AgNPs) was studied in methanol and ethylene glycol by steady state fluorescence measurements. The Stern - Volmer quenching rate constant (K_{sv}) was calculated as 8.1×10^{8} and 8.22×10^{8} M^{-1} in methanol and ethylene glycol respectively. Taking the fluorescence lifetime of BDPD in the absence of silver nanoparticles as 3.2 ns, the values of the fluorescence quenching rate constants ($k_q=K_{sv}/\tau$) are calculated as 2.54×10^{17} and 2.56×10^{17} M^{-1} s^{-1} in methanol and ethylene glycol respectively. From the data, fluorescence resonance energy transfer and / or electron transfer processes play a major role in the fluorescence quenching of BDPD by AgNPs in methanol and low concentrations of Ag NPs in ethylene glycol. The static quenching rate constant in ethylene glycol was calculated by modified Stern - Volmer equation as $V=8.86\times10^{9}$ M^{-1} . For dynamic quenching, the radius of quenching sphere volume r values were found to be 68.3 and 70.6 nm in ethanol and ethylene glycol, respectively. For static quenching in ethylene glycol the effective radius of quenching sphere action (kinetic radius) was calculated as $r=152$ nm.

Keywords N,N-Bis(2,6-dimethylphenyl)-3,4:9,10-perylene-tetracarboxylic diimide · Fluorescence quenching · Silver nano-particles

S. A. El-Daly (✉) · M. A. Hussein · A. M. Asiri
Chemistry Department, Faculty of Science, King Abdulaziz University, P.O. Box 80203, Jeddah 21589, Saudi Arabia
e-mail: samyeldaly@yahoo.com

M. A. Hussein · A. M. Asiri
Center of Excellence for Advanced Materials Research (CEAMR), King Abdulaziz University, Jeddah 21589, P.O. Box 80203, Saudi Arabia

S. A. El-Daly · I. A. Salem
Chemistry Department, Faculty of Science, Tanta University, Tanta, Egypt

M. A. Hussein
Chemistry Department, Faculty of Science, Assiut University, Assiut 71516, Egypt

Introduction

The rapid development of nanotechnology over the last several decades has opened new possibilities for investigating the interaction between photo-excited molecules and metallic nanoparticles. Thus, in recent years there has been a growing interest in the interactions of fluorophores with metallic nanostructures or nanoparticles [1]. The spectral properties of fluorophores can be dramatically modified by near-field interactions with the electron clouds present in metals. These interactions modify the emission in ways not seen in ensemble fluorescence experiments [2]. The type, size and shape of the metallic nanoparticles can modulate the fluorescence of a target dye close to the metal surface. The enhancement of fluorescence efficiency due to electronic coupling of the electronic transition dipole moment with surface Plasmon is a desirable effect owing to the use of medium to low-quantum yield fluorophores in molecular probing devices [3, 4]. The quenching of organic fluorophores by small molecules is thought to arise from dynamic quenching [5–7]. Other reports conclude that both dynamic and static mechanisms are involved in the quenching process [8–10]. Interactions between fluorophores and noble nanoparticles have been investigated

intensively in recent years due to important applications in optical materials, biosensing and scanning probe micrroscopy [11].

Perylene has been widely used as a dye molecule [12–14], because of its high fluorescence quantum yield and chemical stability. The intimate packing of perylene molecules provides rich photophysical and photochemical properties that are important for many technological applications [15, 16]. N-annulation of perylene [17–19] where nitrogen atoms are annulated at the bay position offer improved solubility because flexible alkyl chains can be easily introduced. In addition, the electron-donating character of amines increases the electron density of the entire p-system loading to new optoelectronic properties. Furthermore, Ong et al. reported that the introduction of nitrogen atoms can significantly increase material stability [20]. On the other hand, based on their large p-conjugated system, perylene derivatives possess excellent chemical, thermal, and optical stabilities, and broad absorption and photoconductive properties. Perylene derivatives can also be self-assemble to form a liquid-crystalline phase [21] and are therefore widely used as organic light emitting diodes, fluorescent chemosensors, liquid crystal displays, organic solar cells, and organic field-effect transistors [22–26]. Furthermore, 3,4:9,10-perylenetetracarboxylic dianhydride is the archetypal p stacking organic perylene dye with desirable electronic and optical properties [27, 28]. BDPD is an important highly photostable probe molecule and to the best of our knowledege, there is no any report on fluorescence quenching of BDPD by silver nanoparticles. In the present work, we studied fluorescence quenching by silver nanoparticles in methanol and ethylene glycol in order to determine the mechanism of energy transfer from BDPD to Ag nanoparticles

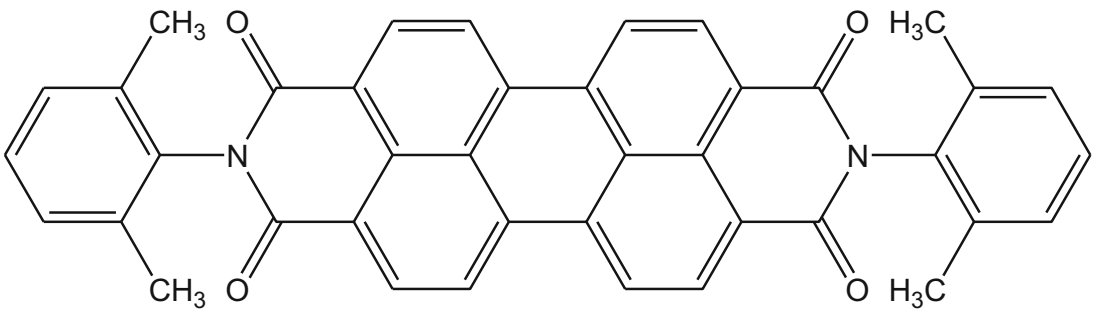

BDPD

Experimental

N,N-bis(2,6-dimethylphenyl)-3,4:9,10-perylenetetracarboxylic diimide (BDPD) was used as received from Aldrich. All solvents used in this work were of spectroscopic grade. Silver nitrate ($AgNO_3$) was purchased from *Sigma-Aldrich*. Citrate trisodium salt (95 %, $C_6H_5O_7Na_3.2H_2O$), hydrochloric and nitric acids were purchased from *Fluka*. All glassware and magnetic stirring beads were cleaned prior to use with freshly prepared aqua regia (1:3 HNO_3: HCl) followed by rinsing with doubly distilled water.

Silver nanoparticles (AgNPs) were prepared by a chemical reduction technique using tri-sodium citrate as surfactant. In a typical synthetic procedure, 50.0 ml of 0.01 M silver nitrate ($AgNO_3$) was stirred with 0.1 M trisodium citrate volume at room temperature for 10 min. To this mixture, 50.0 ml of a 0.1 M solution of ice-cold reducing agent ($NaBH_4$) was added drop-wise and the resulting mixture was stirred for 20 min. After about 10 min, the original transparent solution of silver nitrate and trisodium citrate turned pale-yellow and finally to a light-golden yellow color indicating the formation of aggregated silver nanoparticles. The morphology, size, and structure of silver nanoparticles (AgNPs) were recorded on FE-SEM instrument (JSM-7600F, Japan). A typical solution of 39 nm diameter silver nanoparticles exhibiting a characteristic surface Plasmon band around 431 nm was obtained.

Steady state emission spectra were measured with a Shimadzu RF 5300 spectrofluorometer using a rectangular quartz cell of dimensions 0.2×1.0 cm to minimize reabsorption effect. UV-visible electronic absorption spectra were measured using a Shimadzu UV-visible 1650-pc spectrophotometer.

Results and Discussion

Figure 1a shows the TEM image of the prepared silver NPs, confirms the nanoscale dimension of the particles and shows

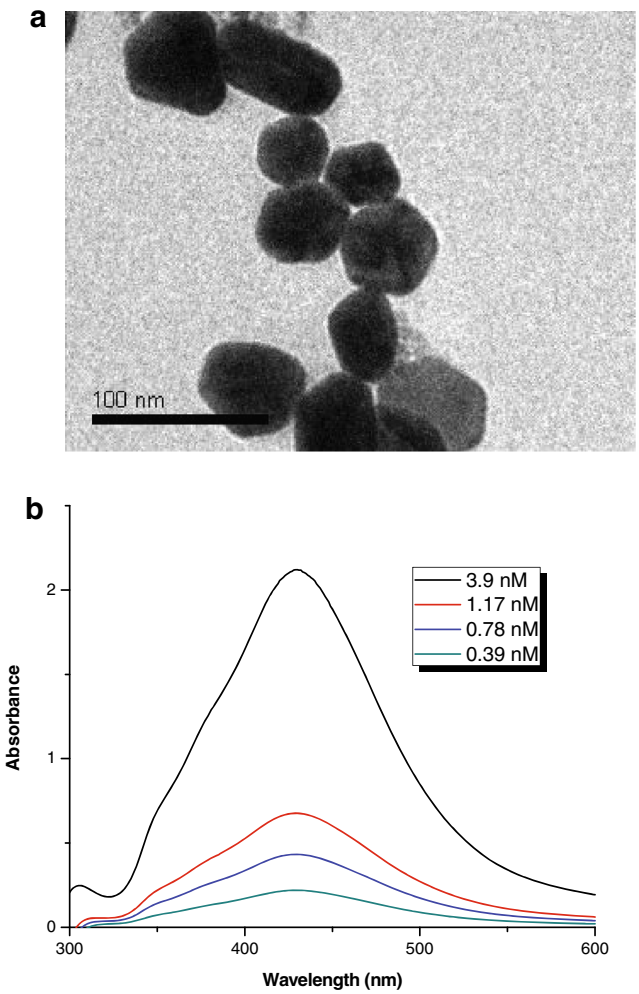

Fig. 1 **a** TEM image of Ag NPs. **b**: Electronic absorption spectra of different concentrations of Ag NPs

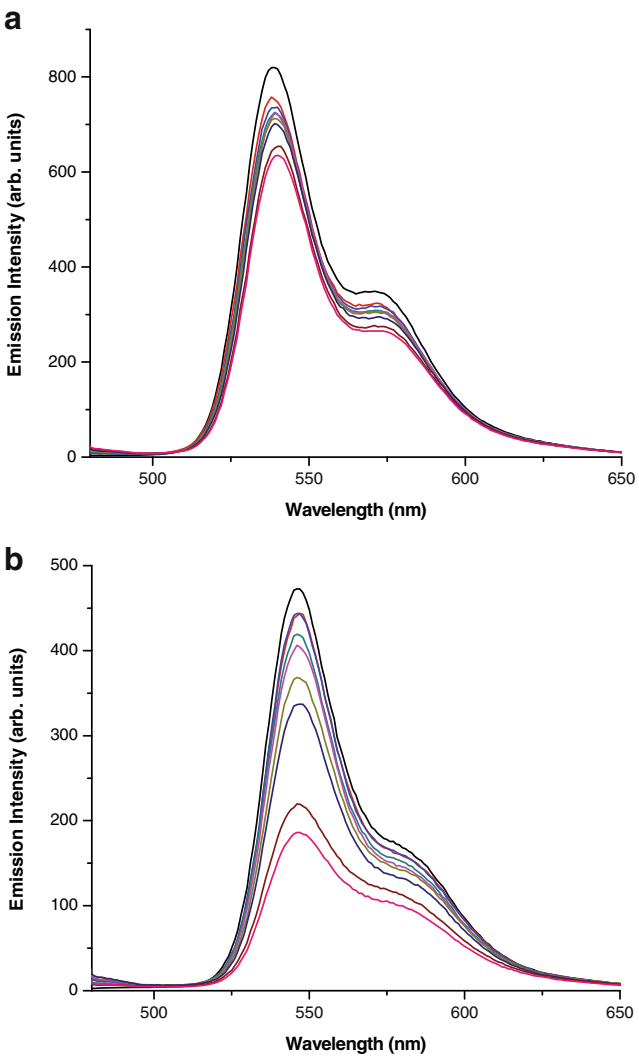

Fig. 2 Emission spectra of 1×10^{-5} mol dm^{-3} solution of BDPD in **a** methanol and **b** ethylene glycol in different concentrations of Ag NPs. The concentrations of Ag NPs at decreasing emission intensity are: 0.00, 0.03, 0.078, 0.117, 0.156, 0.195, 0.234, 0.273 and 0.312 nM, (λ_{ex}= 480 nm)

that the particles have an average diameter of about 39 nm. The electronic absorption spectra of different concentrations (0.39, 0.78, 1.17 and 3.9 nM) of the prepared silver NPs used in the study are shown in Fig. 1b. The fluorescence emission of BDPD was studied in presence of various concentrations of silver NPs in MeOH and ethylene glycol at room temperature. The fluorescence emission of BDPD exhibits a maximum at 530 nm upon excitation at 480 nm. As the concentration of the quencher (Ag NPs) increases, the position of the fluorescence bands of BDPD remains unchanged despite the substantial decrease in the fluorescence intensity as shown in Fig. 2a, b. This indicates the absence of molecular aggregation under the prevailing experimental conditions. No such quenching of BDPD was observed in the presence of low concentrations of capping agent indicating that the silver nanoparticles are responsible for the fluorescence quenching. When the absorption spectra of 1×10^{-5} M **BDPD** were recorded after addition of 1.17 nM Ag NPs in methanol or ethylene glycol, the spectral pattern and absorption maxima remained unchanged. This observation suggests that the fluorophore-quencher interaction does not change the spectral absorption properties of both fluorophore and quencher and there is no observable photochemical reaction between fluorophore and quencher [29].

Figure 3a, b shows the Stern-Volmer plot (derived from Eq. (1)) of BDPD fluorescence quenching using silver nanoparticles as quencher [30].

$$\frac{I_o}{I} = 1 + K_{sv}[Ag] \quad (1)$$

where Io and I are the fluorescence intensities in the absence and presence of the quencher AgNPs. The Stern-Volmer plots of the quenching process of BDPD by Ag NPs in MeOH and ethylene glycol (Fig. 3a, b) show different behavior, a

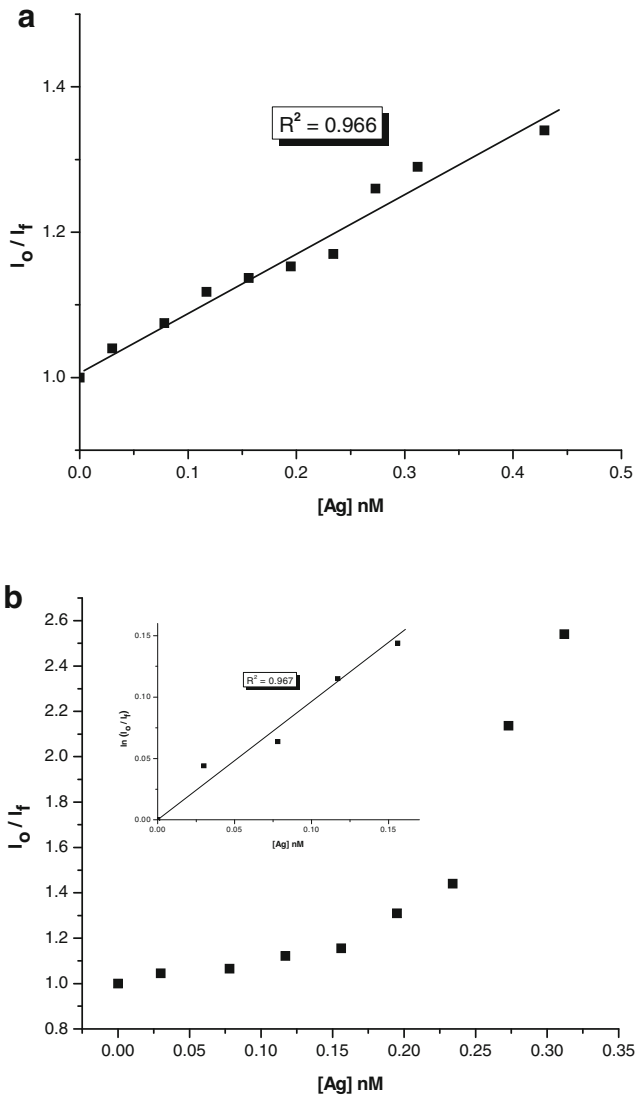

Fig. 3 Stern-Volmer plot of fluorescence quenching of 1×10^{-5} mol dm^{-3} BDPD by Ag NPs in: **a** methanol and **b** ethylene glycol, (λ_{ex}=480 nm)

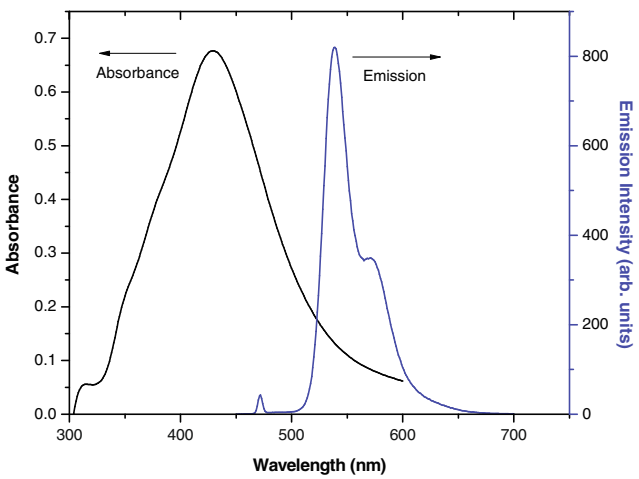

Fig. 4 Electronic absorption spectrum of 1.17 nM of Ag NPs and emission spectrum of 1×10^{-5} mol dm^{-3} solution of BDPD

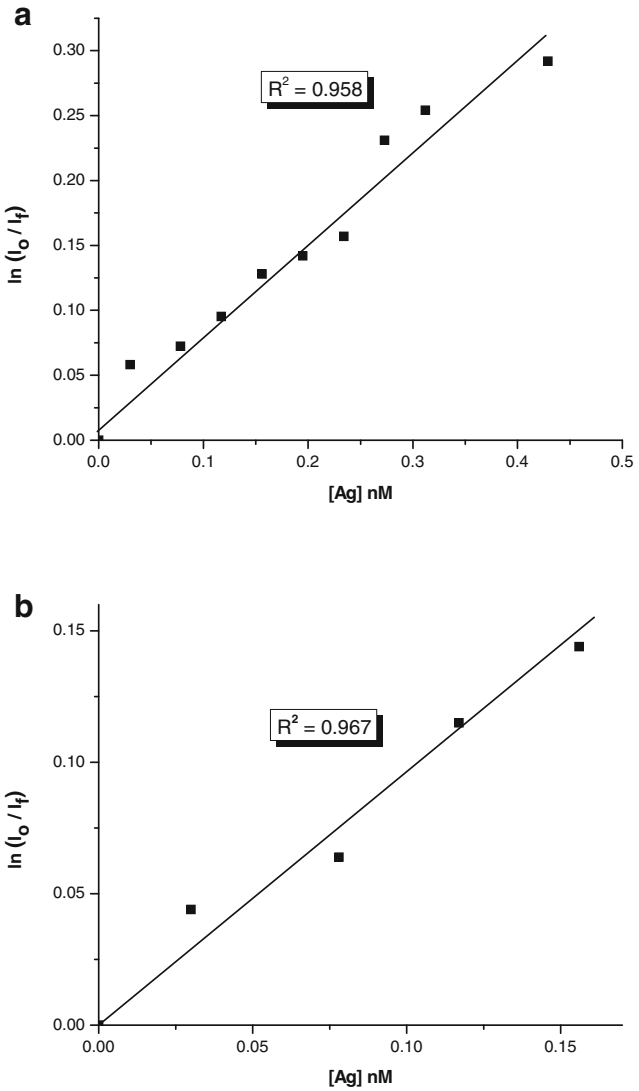

Fig. 5 Perrin plot of fluorescence quenching of 1×10^{-5} mol dm^{-3} BDPD by Ag NPs in: **a** methanol and **b** ethylene glycol, (λ_{ex}=480 nm)

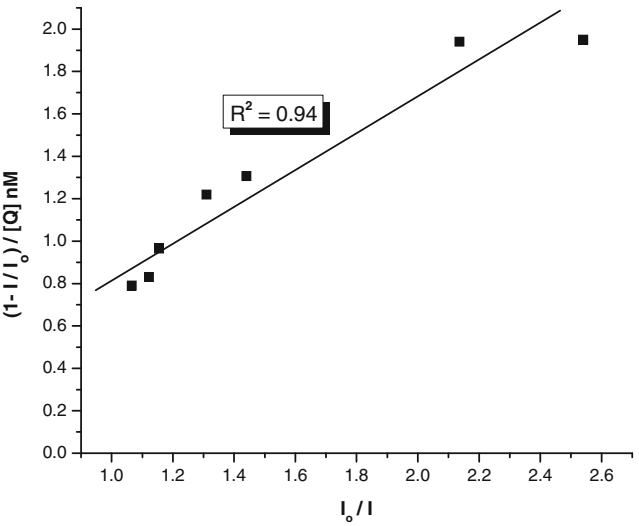

Fig. 6 Plot of modified stern-volmer equation of fluorescence quenching of 1×10^{-5} mol dm^{-3} BDPD by Ag NPs in ethylene glycol

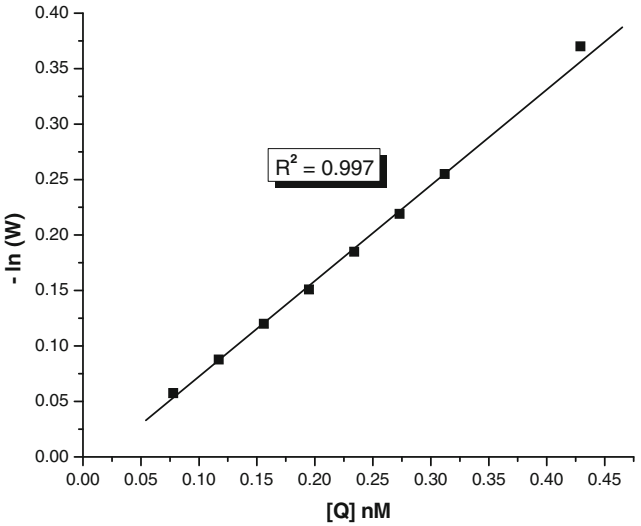

Fig. 7 Plot of *ln W* against [Q] of fluorescence quenching of 1×10^{-5} mol dm^{-3} BDPD by Ag NPs in ethylene glycol

linear correlation in methanol but non linear in ethylene glycol.

From the linear plot and linear portion of the Stern-Volmer plots shown in Fig. 3a, b, the values of K_{SV} in methanol and in ethylene glycol were calculated as 8.1×10^{8} and 8.5×10^{8} M^{-1} in methanol and ethylene glycol, respectively. The bimolecular quenching rate constant (k_q) was calculated as $k_q=2.54\times10^{17}$ and 2.56×10^{17} M^{-1} s^{-1} where, $K_{SV}=k_q\,\tau_f$; taking lifetime of BDPD as $\tau_f=3.2$ *ns* in methanol [31]. These values are much higher than the diffusion rate constant k_d ($k_d=9.2\times10^{10}$ M^{-1} for ethanol and 5.8×10^{8} M^{-1} for ethylene glycol). This suggests fluorescence resonance energy transfer and / or electron transfer processes play a major role in quenching the fluorescence of BDPD by Ag NPs due to a significant overlap between electronic absorption of Ag NPs and the emission of BDPD(Fig. 4). Thus a long range energy transfer is obeyed due to coupling of the electronic transition dipole moment of BDPD with surface Plasmon of Ag. The large values of k_q suggest the existence of strong dipole-dipole interactions between excited sate BDPD and the Plasmon absorption band of AgNps.

The Perrin-model is valid for energy transfer between donor–acceptor components unable to change spatial position with respect to each other on the time scale of the quenching process. The Perrin relationship [32, 33] is given by Eq. (2):

$$\ln\left(\frac{I_o}{I}\right) = VN_o[Q] \tag{2}$$

where I_o and I are emission intensities in the absence and presence of quencher, V is the volume of the quenching sphere in cubic centimeters, N_o is the Avogdaro's number, [Q] is the molar concentration of the quencher, and r is the radius of quenching sphere volume. A plot of $\ln(\frac{I_o}{I})$ versus [Q] (Fig. 5a, b) demonstrats linear behavior with slope equal to VN_o and the V values were found to be 1.34×10^{-15} (r= 68.3 nm) and 1.48×10^{-15} cm^3 (r=70.6 nm) in ethanol and ethylene glycol, respectively.

The nonlinear plot in ethylene glycol showed positive deviation as was observed earlier [34]. The positive deviation from linearity suggests that the quenching is not purely static or purely dynamic, and may be due to simultaneous dynamic and static quenching mechanisms. Analysis of the data was carried out by employing the sphere of action static model using a modified form of Stern-Volmer Eq. (3) [34] given as:

$$\left(\frac{I_o}{I}\right) = \frac{1}{W}(1 + K_{sv}[Q]) \tag{3}$$

Where W is expressed as:

$$W = e^{-V[Q]} \tag{4}$$

and where, 'V' is the static quenching constant that represents an active volume element surrounding the fluorophore in its excited state. Since W depends on the quencher concentration [Q], the S-V plots for a quencher with high quenching

Scheme 1 Illustration of the fluorescence quenching

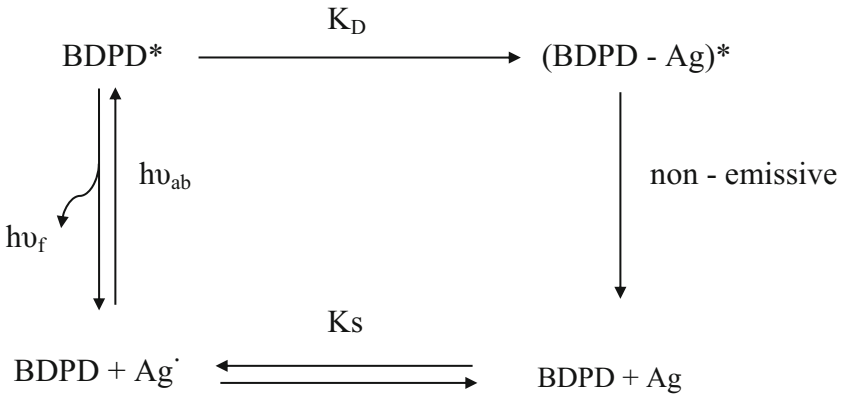

ability generally deviate from linearity. Thus, Eq. (3) is rewritten as:

$$\frac{1-\left(\frac{I}{I_o}\right)}{[Q]} = K_{sv}\left(\frac{I_o}{I}\right) + \frac{1-W}{[Q]} \quad (5)$$

According to Eq. (5), $\frac{1-\left(\frac{I}{I_o}\right)}{[Q]}$ was plotted against $\left(\frac{I_o}{I}\right)$ (Fig. 6) and the S-V dynamic quenching constant, K_{SV}, was obtained by a least-square fit to determine the slope, $K_{SV}=0.822\times 10^8\ M^{-1}$. The intercept of the plot was used to calculate *W* values for each quencher concentration [Q]. A plot of *ln W* against [Q] was linear correlation with negative slope (Fig. 7) to give the static quenching constant '**V'**$=8.86\times10^9\ M^{-1}$. From the value of '*V*', the effective quenching radius of the sphere of action (kinetic distance) '*r was calculated as* 1520 (152 nm) ($V = \frac{4}{3}\pi r^3 \times \frac{N}{1000}$). The radius of the BDPD dye (R_d) was determined using the additive model of Edward [35] as $R_d=5.2$. The sum of the molecular radii, i.e. 'encounter distance', $R=R_d+R_{Ag}$ is determined as 200.2 . We noted that the value of the kinetic distance *'r'* was greater than the encounter distance *R.* Therefore, according to Andre [36] and Zeng [37], the static effect occurs irrespective of the ground state complex formation provided the reactions are diffusion limited indicating that the sphere of action model holds. It may also be noted that a positive deviation in the S-V plot is expected when both static and dynamic quenching occur simultaneously [34, 38]. Scheme 1 illustrates the possible interaction between BDPD and AgNPs in ethylene glycol where Ks and K_D are the static and dynamic quenching rate constants.

Conclusion

BDPD displays fluorescence quenching by colloidal AgNPs in methanol and ethylene glycol. From the quenching data, energy transfer and static quenching from excited dye to AgNPs play major role in the quenching of DBPI fluorescence by AgNPs. The dynamic quenching rate constants are calculated as 8.1×10^8 and $8.22\times10^8\ M^{-1}$ in methanol and ethylene glycol respectively. The second order fluorescence quenching rate constants ($k_q=K_{sv}/\tau$) are caculated as 2.54×10^{17} and $2.56\times10^{17}\ M^{-1}\ s^{-1}$ in methanol and ethylene glycol respectively. By application of the modefided Stern - Volmer equation of fluorescence quenching in ethylene glycol, the static quenching rate constant is calculated as $V=8.86\times10^9\ M^{-1}$. The effective quenching radius of the sphere of action(kinetic distance) '*r is found to be* 1520 (152 nm).

References

1. Thomas KG, Kamat PV (2003) Chromophore-functionalized gold nanoparticles. Acc Chem Res 36:888–898
2. Fu Y, Lakowicz JR (2009) Modification of single molecule fluorescence near metallic nanostructures. Laser Photonics Rev 3:221–232
3. Zhang J, Matveeva E, Gryczynski I, Leonenko Z, Lakowicz JR (2005) Metal-enhanced fluoroimmunoassay on a silver film by vapor deposition. J Phys Chem B 109:7969–7968.
4. Zhang J, Malicka J, Gryczynski I, Lakowicz JR (2005) Surface-enhanced fluorescence of fluorescein-labeled oligonucleotides capped on silver nanoparticles. J Phys Chem B 109:7643–7648.
5. Corrigan TD, Guo S, Phaneuf RJ, Szmacinski H (2005) Enhanced fluorescence from periodic arrays of silver nanoparticles. J Fluoresc 15:777–784.
6. Haes AJ, Stuart AD, Nie S, Van Duyne RP (2004) Using solution-phase nanoparticles, surface-confined nanoparticle arrays and single naanoparticles as biological sensing platforms. J Fluoresc 14:355–367.
7. Kotiaho A, Lahtinen R, Latvala H, Efimov A, Tkachenko NV, Lemmetyinen H (2009) Effect of gold nanoparticles on intramolecular exciplex emission in organized porphyrin–fullerene dyad films. Chem Phys Lett 471:269–275.
8. Pramanik S, Bhattacharya SC, Imae T (2007) Fluorescence quenching of 3,7-diamino-2,8-dimethyl-5-phenyl phenazinium chloride by AgCl and Ag nanoparticles. J Lumin 126:155–159.
9. Landes CF, Braun M, El-Sayed MA (2001) On the nanoparticle to molecular size transition: fluorescence quenching studies. J Phys Chem B 105:10554–10558.
10. Lee IS, Suzuki H (2008) Quenching dynamics promoted by silver nanoparticles. J Photochem Photobiol A Chem 195:254–260.
11. Lakowicz JR (2006) Principles of fluorescence spectroscopy, 3rd edn. Springer, New York, Chapter 8
12. Donaldson DM, Robertson JM, White JG (1964) Proc Roy Soc London A279:129
13. Tanaka J (1963) The electronic spectra of aromatic molecular crystals. II. The crystal structure and spectra of perylene. Bull Chem Soc Jpn 36:1237–1249.
14. Chu NYC, Kearns DR (1972) Monomer emission from excimer forming crystals: pyrene and perylene. Mol Cryst Liq Cryst 16:61–74.
15. Weiss D, Kietzmann R, Mahrt J, Tufts B, Storck W, Willig F (1992) E-excimer and Y-type luminescence of perylene dimers in a Langmuir-Blodgett film at 1.5 K. J Phys Chem 96:5320–5325.
16. Akimoto S, Ohmori A, Yamazaki I (1997) Dimer formation and excitation relaxation of perylene in Langmuir−Blodgett films. J Phys Chem B 101:3753–3758.
17. Zhen Y, Qian H, Xiang J, Qu J, Wang Z (2009) Highly regiospecific synthetic approach to monobay-functionalized perylene bisimide and di(perylene bisimide). Org Lett 11:3084–3087.
18. Li Y, Wang Z (2009) Bis-N-annulated quaterrylene: an approach to processable graphene nanoribbons. Org Lett 11:1385–1387.
19. Chen H, He C, Yu G, Zhao Y, Huang J, Zhu M, Liu H, Guo Y, Li Y, Liu Y (2012) Phenanthro[1,10,9,8-cdefg]carbazole-containing copolymer for high performance thin-film transistors and polymer solar cells. J Mater Chem 22:3696–3698.
20. Wu Y, Li Y, Ong BS (2007) A simple and efficient approach to a printable silver conductor for printed electronics. J Am Chem Soc 129:1862–1863.
21. Kufazvinei C, Ruether M, Wang J, Blau W (2009) A blue light emitting perylene derivative with improved solubility and aggregation control: Synthesis, characterisation and optical limiting properties. Org Electron 10:674–680.
22. Haas U, Thalacker C, Adams J, Fuhrmann J, Riethmuller S, Beginn U, Ziener U, Möller M, Dobrawaa R, Würthner F (2003) Fabrication

and fluorescence properties of perylene bisimide dye aggregates bound to gold surfaces and nanopatterns. J Mater Chem 13:767–772.
23. He X, Liu H, Li Y, Wang S, Wang N, Xiao J, Xu X, Zhu D (2005) Gold nanoparticle-based fluorometric and colorimetric sensing of copper(II) Ions. Adv Mater 17:2811–2815.
24. Keuker-Baumann S, Bock H, Sala FD, Benning SA, Haßheider T, Frauenheim T, Kitzerow H-S (2001) Absorption and luminescence spectra of electroluminescent liquid crystals with triphenylene, pyrene and perylene units. Liq Cryst 28:1105–1113.
25. Shi M-M, Chen H-Z, Sun J-Z, Ye J, Wang M (2003) Fluoroperylene diimide: a soluble and air-stable electron acceptor. Chem Commun 14:1710–1711.
26. Horowitz G, Kouki F, Spearman P, Fichou D, Nogues C, Pan X, Garnier F (1996) Evidence for n-type conduction in a perylene tetracarboxylic diimide derivative. Adv Mater 8:242–245.
27. Bulovic V, Forrest SR (1996) Study of localized and extended excitons in 3,4,9,10-perylenetetracarboxylic dianhydride (PTCDA) II. Photocurrent response at low electric fields. Chem Phys 210:13–25.
28. Forrest SR (1997) Ultrathin organic films grown by organic molecular beam deposition and related techniques. Chem Rev 97:1793–1896.
29. Frens G (1973) controlled nucleation for the regulation of the particle size in monodisperse Gold Suspensions. Nat Phys Sci 241:20–22.
30. Amjadi M, Farzampour L (2014) Fluorescence quenching of fluoroquinolones by gold nanoparticles with different sizes and its analytical application. J Lumin 145:263–268.
31. El-Daly SA (1999) Spectral, lifetime, fluorescence quenching, energy transfer and photodecomposition of N, N′-bis(2,6-dimethyl phenyl)-3,4:9,10-perylentetracarboxylic diimide (DXP). Spectrochim Acta A 55:143–152.
32. Penzer GR (1980) In: Brown SB (ed) An introduction to spectroscopy for biochemists, vol 68. Academis Press, London
33. Shelli R, Coffer JL (1992) Deactivation of Q-cadmium sulfide photoluminescence through polynucleotide surface binding. J Phys Chem 96:10581–10584.
34. Hanagodimath SM, Manohara SR, Biradar DS, Hadimani SKB (2008) Fluorescence Quenching of 2,2″-dimethyl-p-terphenyl by Carbon Tetrachloride in Binary Mixtures. Spectrosc Lett 41:242–250.
35. Edward JT (1956) "Molecular volumes and parachor". Chem Ind, London, p. 774
36. Andre JC, Niclause M, Ware WR (1978) Kinetics of partly diffusion controlled reactions. I. Transient and apparent transient effect in fluorescence quenching. Chem Phys 28:371–377.
37. Zeng H, Durocher G (1995) Analysis of fluorescence quenching in some antioxidants from non-linear Stern—Volmer plots. J Lumin 63: 75–84.
38. Melavanki RM, Kusanur RA, Kadadevaramath JS, Kulakarni MV (2009) Quenching mechanisms of 5BAMC by aniline in different solvents using Stern–Volmer plots. J Lumin 129: 1298–1303.